J. Fluid Mech. (2006), *vol.* 568, *pp.* 329–349.
doi:10.1017/S0022112006002424 Printed in the United Kingdom

Bifurcation of vortex breakdown patterns in a circular cylinder with two rotating covers

By MORTEN BRØNS AND ANDERS V. BISGAARD

Department of Mathematics, Technical University of Denmark, DK-2800 Kongens Lyngby, Denmark

(Received 28 July 2005 and in revised form 18 May 2006)

We analyse the topology of vortex breakdown in a closed cylindrical container in the steady domain under variation of three parameters, the aspect ratio of the cylinder, the Reynolds number, and the ratio of the angular velocities of the covers. We develop a general post-processing method to obtain topological bifurcation diagrams from a database of simulations of two-dimensional flows and apply the method to axisymmetric simulations of the flow in the cylinder. Interpreting the diagrams with the aid of bifurcation theory, we obtain complete topological bifurcation diagrams for the rotation ratio in the interval [−0.04, 0.075]. In this narrow range we identify three codimension-3 bifurcation points which act as organising centres for the entire bifurcation diagram.

1. Introduction

In many vortex flows, secondary flow structures in the form of recirculating zones may develop on the vortex axis. Such zones, or *vortex breakdown bubbles*, appear for instance in the flow in a cylinder driven by rotating covers. The parameters characterizing the flow are the cylinder aspect ratio h, the rotational Reynolds number Re and the ratio of the angular velocities of the top and bottom lids γ given by

$$h = \frac{H}{R}, \qquad Re = \frac{\Omega_1 R^2}{\nu}, \qquad \gamma = \frac{\Omega_2}{\Omega_1}, \tag{1}$$

where R and H are the radius and height of the cylinder, Ω_1 and Ω_2 are the angular velocities of the rotating covers and ν is the kinematic viscosity of the fluid.

Vogel (1968), Ronnenberg (1977) and Escudier (1984) have conducted experiments in the steady-flow regime for one fixed cover, corresponding to $\gamma = 0$, and have examined the parameter domain $1.0 \leqslant h \leqslant 2.5$ and $1000 \leqslant Re \leqslant 3000$, locating regimes with up to three recirculation bubbles. Numerical simulations assuming the flow is axisymmetric, e.g. by Sørensen & Loc (1989), Lopez (1990), Daube (1991) and Tsitverblit (1993), reproduce the overall flow structure from experiments well, although the details of the bubble structure are influenced by asymmetric perturbations induced by imperfections in the experimental set-up (Spohn, Mory & Hopfinger 1998; Sotiropoulos & Ventikos 2001; Hartnack, Brøns & Spohn 2000; Thompson & Hourigan 2003). It is clearly established that the creation of recirculation bubbles is not associated with a hydrodynamic instability. In the range we consider, there is a unique steady stable solution to the Navier–Stokes equations. The creation of the bubbles is a change of the topology of that steady solution. At higher Re, the steady solution loses stability to an oscillating flow in a Hopf bifurcation (Tsitverblit 1993; Gelfgat, Bar-Yoseph & Solan 1996*b*, 2001).

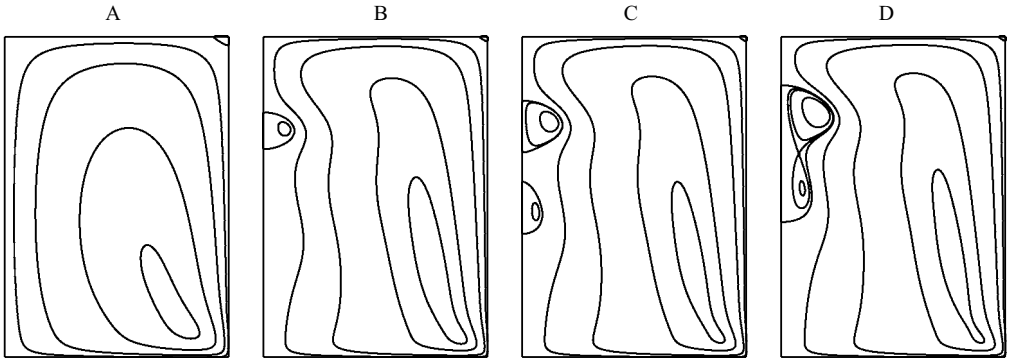

FIGURE 1. Typical representatives of the four topologies (iso-curves of the stream function ψ) we observe in the present study, here for $\gamma = 0.012$ and $h = 2.2$. Only the right-hand half of the meridional plane is shown. The vertical line to the left is the cylinder axis. A: $Re = 700$, no bubbles. B: $Re = 1680$, one bubble. C: $Re = 1800$, two bubbles. D: $Re = 2080$, one bubble with inner structure.

Numerical and experimental studies for $\gamma \neq 0$ have been performed by Bar-Yoseph, Solan & Roesner (1990*a*, *b*), Valentine & Jahnke (1994), Gelfgat, Bar-Yoseph & Solan (1996*a*), Brøns, Voigt & Sørensen (1999, 2001) and Okulov, Sørensen & Voigt (2005). The number and structure of the breakdown bubbles turn out to be very sensitive to variations in γ. This sensitivity indicates the possibility for control of vortex breakdown in the flow. Mununga *et al.* (2005) show that vortex breakdown can be controlled by a small rotating disk at the top and Herrada & Shtern (2003) control vortex breakdown by temperature gradients. A new interest in the flow and its control stems from its potential use as a bioreactor (Dusting, Sheridan & Hourigan 2004).

Using methods from dynamical systems theory, Brøns *et al.* (1999) initiated a systematic construction of topological bifurcation diagrams in the steady regime. Only the range $-0.02 \leqslant \gamma \leqslant 0.05$ was considered, and it is the purpose of the present paper to extend the results to cover a larger range of rotation ratios. To this end, we propose a general post-processing method, the *isocline method*, to obtain topological bifurcation diagrams from numerical simulations of two-dimensional incompressible flows.

Here we cover the range $-0.04 \leqslant \gamma \leqslant 0.075$. It may still seem narrow, but was chosen to demonstrate the applicability of the isocline method and because it contains a surprisingly large set of different bifurcation phenomena involving the flow topologies depicted in figure 1. Through the analysis, we see how the two-bubble parameter range is created and disappears again.

The theory of dynamical systems is useful not only for deriving the isocline method as a post-processing tool; it also serves as a guideline to interpret the numerically obtained bifurcation diagrams. We will show that the bifurcation structure in the three-dimensional parameter space is completely described by the theory of bifurcation of stagnation points close to the cylinder axis (Brøns 1999, 2006). In particular, we determine the existence of three *codimension-3* points $(h^{(i)}, Re^{(i)}, \gamma^{(i)})$, $i = 1, 2, 3$ in the parameter space. Close to these points, the bifurcation structure is well understood from the theory, and the complete bifurcation structure can qualitatively be seen as a patching together of the local bifurcation diagrams.

Parts of the present work have been announced previously (Brøns & Bisgaard 2004).

2. Computational method for the flow in the cylinder

The radial and axial components (u, v) of the incompressible axisymmetric velocity field in the cylindrical container may be described by a stream function ψ such that

$$u = \frac{1}{r}\frac{\partial \psi}{\partial y}, \qquad v = -\frac{1}{r}\frac{\partial \psi}{\partial r}. \tag{2}$$

Here r, y are the radial and axial variables, respectively. Introducing $x = r^2/2$, the differential equations for the curves intersecting the stream surfaces in a meridional plane are

$$\frac{\mathrm{d}x}{\mathrm{d}t} = u = \frac{\partial \psi}{\partial y}, \qquad \frac{\mathrm{d}y}{\mathrm{d}t} = v = -\frac{\partial \psi}{\partial x}. \tag{3}$$

The topology of the iso-curves of ψ is determined by a qualitative study of the trajectories of the non-linear system of differential equations (3). These equations are also obtained for the streamlines for a two-dimensional incompressible flow in Cartesian coordinates, and hence the same topological methods can be applied in both cases.

To compute the stream function for the axisymmetric flow in the cylindrical container we employ the finite-difference solver *czax* developed at LIMSI/CNRS in France (Daube *et al.* 1985; Sørensen & Loc 1989; Daube 1991). The code has been validated against experiments by Sørensen & Loc (1989), Westergaard, Buchhave & Sørensen (1993), and Sørensen & Christensen (1995). It was found that simulations with a grid resolution of $\Delta r = \Delta y = 0.01$ reproduce experiments accurately. Brøns *et al.* (1999, 2001) investigated the influence of the grid size on the accuracy of the determination of topological bifurcation points. Again, $\Delta r = \Delta y = 0.01$ gave satisfactory results, and this grid size will also be employed here. We consider the parameter range $0 \leqslant Re \leqslant 2400$, $0 \leqslant h \leqslant 3$, $-0.040 \leqslant \gamma \leqslant 0.075$, where there is a unique stable steady solution to the Navier–Stokes equations. It is found by performing dynamic simulations until transients have died out.

3. The isocline method for topological bifurcation diagrams

Consider a two-dimensional velocity field (u, v) depending smoothly on Cartesian coordinates (x, y) and a vector $\boldsymbol{p}$ of parameters. For simplicity, we consider here only two scalar parameters, so $\boldsymbol{p} = (p_1, p_2)$.

The basic topological bifurcation of a flow pattern is the change of the number of stagnation points, that is, the points where the velocity vanishes, $u(x, y) = v(x, y) = 0$. To monitor the creation or disappearance of stagnation points, we first locate, for a fixed $\boldsymbol{p}$, the ∞-*isocline*. This is the set of points (x, y) in the flow plane where $u = 0$. Generically, this set consists of a number of curves (branches). Stagnation points can be located by keeping track of v along the ∞-isocline, and finding points where $v = 0$. To formalize this, consider a branch of the ∞-isocline parameterized by arclength s,

$$(x, y) = (x_\infty(s), y_\infty(s)), \tag{4}$$

and consider the variation of v along the branch,

$$V(s) = v(x_\infty(s), y_\infty(s)). \tag{5}$$

Typical graphs of V when $\boldsymbol{p}$ is close to a bifurcation are shown in figure 2. In figure 2(a), V has the same sign everywhere, and there are no stagnation points. As $\boldsymbol{p}$

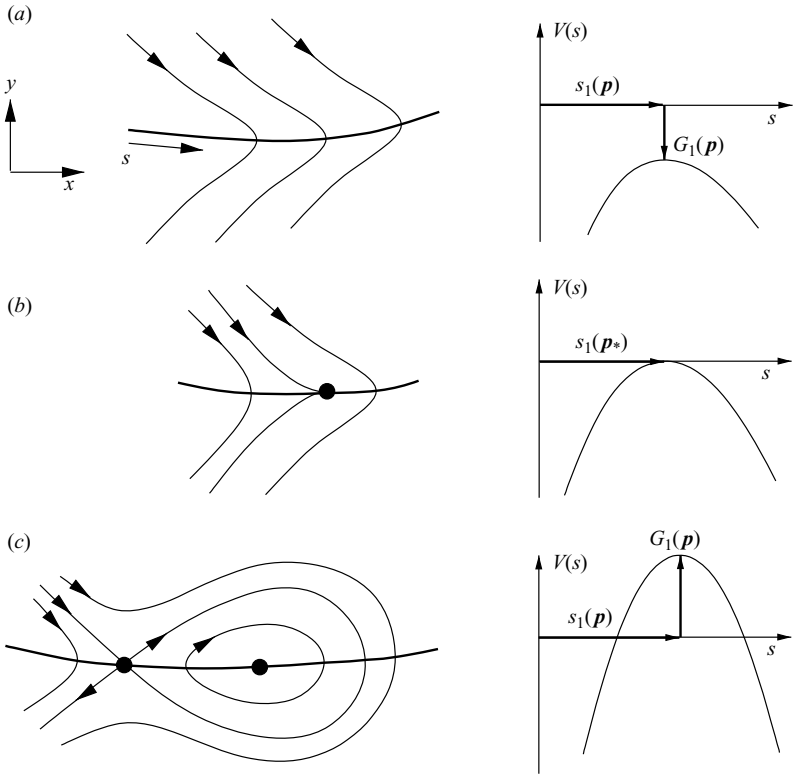

FIGURE 2. The creation of stagnation points in an in-flow cusp bifurcation under variation of parameters $\boldsymbol{p}$ through the bifurcation point $\boldsymbol{p}_*$. The left-hand column shows streamline patterns, stagnation points, and the ∞-isocline (heavy line). The right-hand column shows corresponding graphs of V with a critical point s_1, and the bifurcation function $G_1(\boldsymbol{p})$.

is varied, a local extremum of V takes the value 0 at the bifurcation point $\boldsymbol{p} = \boldsymbol{p}_*$ in figure 2(*b*), and has changed its sign in figure 2(*c*) where two stagnation points exist.

We denote the critical point of V by s_1, that is, $V'(s_1) = 0$. It will depend on the system parameters, $s_1 = s_1(\boldsymbol{p})$. Now define the *bifurcation function*

$$G_1(\boldsymbol{p}) = V(s_1(\boldsymbol{p})). \tag{6}$$

It appears from figure 2 that the bifurcation occurs when

$$G_1(\boldsymbol{p}) = 0. \tag{7}$$

Solving this equation gives bifurcation curves in the parameter space $\mathbb{R}^2$. The critical point s_1 may not exist for all values of $\boldsymbol{p}$. However, under the generic condition that the extremum of V at the bifurcation point $\boldsymbol{p} = \boldsymbol{p}_*$ is quadratic, $V''(s_1(\boldsymbol{p}_*)) \neq 0$, the bifurcation function G_1 is well-defined in a neighbourhood of $\boldsymbol{p}_*$. This is the situation illustrated in figure 2 in a flow region away from boundaries. This bifurcation is known as a *cusp bifurcation.*

There may be several critical points $s_1, s_2, \ldots$ of V, and each gives rise to a bifurcation function G_i, which must be treated individually. Furthermore, the process must be repeated for each branch of the ∞-isocline.

We stress that the bifurcations considered here are not related to any form of hydrodynamic instability. We consider a flow regime where the Navier–Stokes

equations have a unique steady solution which depends smoothly on the external parameters. It is only the topology of the streamlines for this family of steady flows which changes. The dynamical system we consider here is the ordinary differential equations (3), and a determination of the stability of the stagnation points, considered as equilibrium points, can be performed. Since only the flow topology is of interest in the present study, we omit this analysis. If, however, the motion of fluid particles is of interest, for instance in a study of mixing, such a stability analysis is pertinent.

Any bifurcation phenomenon is associated with an integer number, the *codimension* (Wiggins 2003). Topological bifurcations occur when degenerate stagnation points are present in the flow, and the codimension measures the number of degeneracy conditions fulfilled for that stagnation point. The scenario in figure 2 is associated with a single degeneracy condition, namely $V'(s_1(\boldsymbol{p}_*))=0$, and a non-degeneracy condition $V''(s_1(p_*))\neq 0$ and hence has codimension 1. If the non-degeneracy condition is violated, $V''(s_1(\boldsymbol{p}_*))=0$, but a new non-degeneracy condition is fulfilled, $V'''(s_1(\boldsymbol{p}_*))\neq 0$, the bifurcation point has codimension 2. Bifurcation points of codimension 2 occur where curves of codimension-1 bifurcation points meet. Hence, they are important for the understanding of the structure of the bifurcation diagram.

To find bifurcation points of codimension 2, we proceed as follows. Let σ_1 denote a critical point of V', that is, $V''(\sigma_1)=0$. This will depend on $\boldsymbol{p}$, so we can define two functions of the parameters,

$$H_1(\boldsymbol{p}) = V(\sigma_1(\boldsymbol{p})), \qquad K_1(\boldsymbol{p}) = V'(\sigma_1(\boldsymbol{p})). \tag{8}$$

The solutions to $H_1(\boldsymbol{p})=0$ and $K_1(\boldsymbol{p})=0$ are curves in the parameter plane. At a point $\boldsymbol{p}_{**}$ where a pair of these curves intersect, we have

$$V(\sigma_1(\boldsymbol{p}_{**})) = V'(\sigma_1(\boldsymbol{p}_{**})) = V''(\sigma_1(\boldsymbol{p}_{**})) = 0, \tag{9}$$

and hence $\boldsymbol{p}_{**}$ is a codimension-2 bifurcation point. As before, there may be several critical points $\sigma_1, \sigma_2, \ldots$, giving rise to different functions H_i, K_i, which must be treated in turn, as well as the entire procedure for each of the branches of the ∞-isocline.

If more free parameters are present in the problem, more degeneracy conditions may appear by proper choice of the parameters, and bifurcations of higher codimension become relevant. The procedure above can, in principle, be generalized to find bifurcations of any codimension, but as higher-order derivatives of V are required, the numerical computations may become difficult.

In the isocline method, the role of the velocity components u and v may obviously be interchanged. Hence, we may start with the 0-isocline where $v=0$ and keep track of $u=U(s)$ along its branches. For the flow in the cylinder, we will use a combination of both classes of isoclines.

To illustrate the method by a simple analytical example, we consider the flow generated from the stream function

$$\psi = \tfrac{1}{2}y + p_1 x + p_2 x^2 + \tfrac{1}{4}x^4, \tag{10}$$

which was derived by Brøns & Hartnack (1999) as a normal form for two-parameter bifurcation in a general flow. As

$$u(x, y) = y, \quad v(x, y) = -(p_1 + 2p_2 x + x^3), \tag{11}$$

we see that the ∞-isocline has the x-axis as its only branch. We choose $s=x$ as arclength and obtain

$$V(s) = v(s, 0) = -(p_1 + 2p_2 s + s^3). \tag{12}$$

This function has two critical points which are defined for $p_2 \leqslant 0$ only,

$$s_1 = \frac{\sqrt{6}}{3}\sqrt{-p_2}, \qquad s_2 = -\frac{\sqrt{6}}{3}\sqrt{-p_2}. \tag{13}$$

We find the bifurcation functions

$$\left.\begin{aligned} G_1(p_1, p_2) = V(s_1) &= -p_1 + \frac{4\sqrt{6}}{9}(-p_2)^{3/2}, \\ G_2(p_1, p_2) = V(s_2) &= -p_1 - \frac{4\sqrt{6}}{9}(-p_2)^{3/2}, \end{aligned}\right\} \tag{14}$$

and hence the two codimension-1 bifurcation curves

$$p_1 = \frac{4\sqrt{6}}{9}(-p_2)^{3/2}, \qquad p_1 = -\frac{4\sqrt{6}}{9}(-p_2)^{3/2}, \qquad p_2 \leqslant 0. \tag{15}$$

To find codimension-2 bifurcation points, we consider the equation

$$V''(s) = -6s = 0 \tag{16}$$

with the unique solution $\sigma_1 = 0$ and define

$$H_1(p_1, p_2) = V(\sigma_1) = -p_1, \qquad K_1(p_1, p_2) = V'(\sigma_1) = -2p_2. \tag{17}$$

The solution to $H_1 = K_1 = 0$ is $(p_1, p_2) = (0, 0)$. Thus, the two bifurcation curves (15) meet at this unique codimension-2 point. The bifurcation diagram thus obtained agrees with the one found previously (Brøns & Hartnack 1999, figure 4).

4. Numerical post-processing using the isocline method

For the flow in the cylinder, we aim at constructing a series of topological bifurcation diagrams in the (h, Re) parameter plane for fixed values of the rotation ratio γ. To this end, we use the solver described in § 2 to obtain a database of stream functions by computing steady flows for each parameter pair on a rectangular grid in the (h, Re)-plane, typically with $\Delta h = 0.08$ and $\Delta Re = 25$. The stream function is represented as values on the grid points in the (r, y)-plane.

In this section, we describe a numerical implementation of the isocline method as a post-processing method by showing how a part of the bifurcation diagram is obtained from the database of stream functions at $\gamma = 0.012$.

4.1. *On-axis bifurcations*

For the present flow, the cylinder axis is always an ∞-isocline, since the radial velocity vanishes here. The axis is parameterized by $s = y$, $0 \leqslant s \leqslant h$. We start by processing data on this branch.

Note, that in addition to being an isocline, the axis is also a streamline. Thus, the creation of stagnation points on the axis gives rise to slightly different topologies from those depicted in figure 2. We return to a general classification of the flow topologies in § 6.1.

The first step is to partition the parameter plane into regions with the same number of critical points s_i of V. In each region, the critical points can be unambiguously labelled by the order they appear along the axis. Figure 3 shows that there are regions with three, five and seven critical points s_i, labelled F_3, F_5, F_7, respectively. Each of the s_i in each of the regions F_k gives rise to a bifurcation function $G_{i,k}(h, Re) = V(s_i)$. Bifurcation curves are easily found using the MATLAB function *contour*, specifying

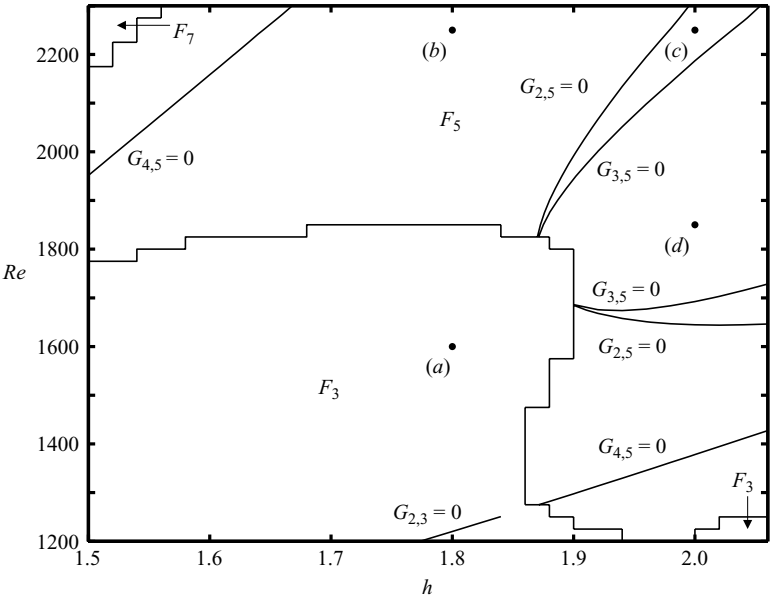

FIGURE 3. The first steps in constructing the bifurcation diagram for $\gamma = 0.012$. The regions F_k are bounded by piecewise linear curves reflecting the stepsize of the parameter grid. The smooth curves are bifurcation curves obtained as zeros of the bifurcation functions. The markers labelled (a)–(d) correspond to the cases shown in figure 4.

the contour level 0. These bifurcation curves are shown in figure 3. It appears that only a few of the bifurcation equations $G_{i,k}(h, Re) = 0$ have a solution.

To illustrate the method and the role of the regions F_k, sample graphs of V and corresponding flow topologies are shown in figure 4. Case (a) is in the region F_3 with three critical points for V. Furthermore, V has two zeros, corresponding to stagnation points on the axis. As shown, these mark the top and bottom of a bubble attached to the axis. Moving to case (b), belonging to F_5, there are five critical points for V, but no change in the topology, as there are still only two zeros of V. Turning to case (c), still in F_5, the sign of $V(s_2)$ has changed, giving rise to two new zeros of V and a new bubble on the axis. Finally, in case (d), $V(s_3)$ has changed sign, corresponding to the merging of the two recirculation bubbles and the creation of a single bubble with an inner structure.

We proceed to find codimension-2 points. To this end, we partition the parameter plane into regions with a constant number of critical points for V'. As shown in figure 5, there are two such regions with six and eight critical points σ_i, respectively. In S_6, only the functions $H_{3,6}$ and $K_{3,6}$ have simultaneous solution curves. These intersect in two codimension-2 points.

4.2. *Off-axis bifurcation*

To locate bifurcations in the cylinder flow off the cylinder axis, we have found it convenient to switch to the 0-isocline. Otherwise we proceed as above, but first the isocline is generated from the (r, y) grid values of v, which is obtained during the *czax* computation in addition to ψ. The MATLAB function *contour* is used to solve $v = 0$. It outputs discrete points on the isocline, separated into branches.

In figure 6, we show a branch of the 0-isocline obtained this way, parameterized as $(x_0(s), y_0(s))$ together with the function $U(s) = u(x_0(s), y_0(s))$. In case (a) (figure 6*a*),

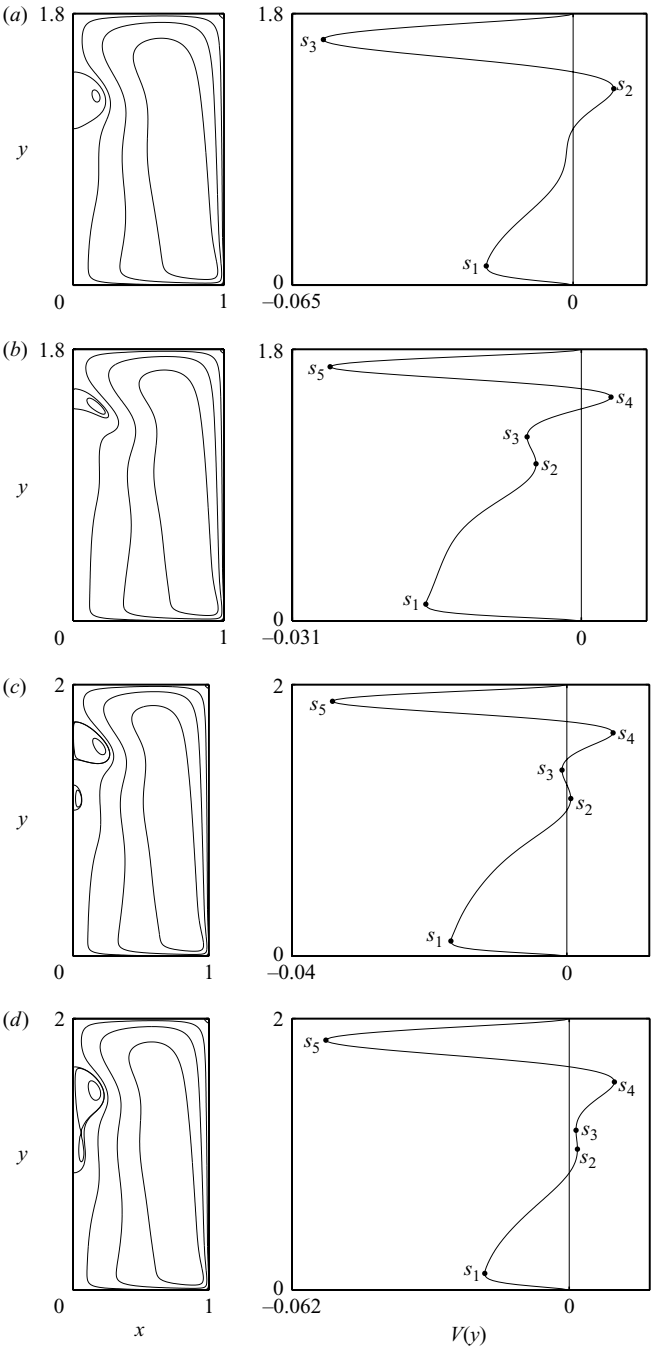

FIGURE 4. Sample flow topologies and corresponding functions V on the cylinder axis for $\gamma = 0.012$. (*a*) $Re = 1600$, $h = 1.8$. (*b*) $Re = 2250$, $h = 1.8$. (*c*) $Re = 2250$, $h = 2.0$. (*d*) $Re = 1850$, $h = 2.0$.

U has two critical points and one zero, corresponding to the single off-axis critical point. As parameters are changed towards case (*d*) (figure 6*b*), two new critical points emerge, and in one of them, s_3, U changes sign, signalling the creation of two new

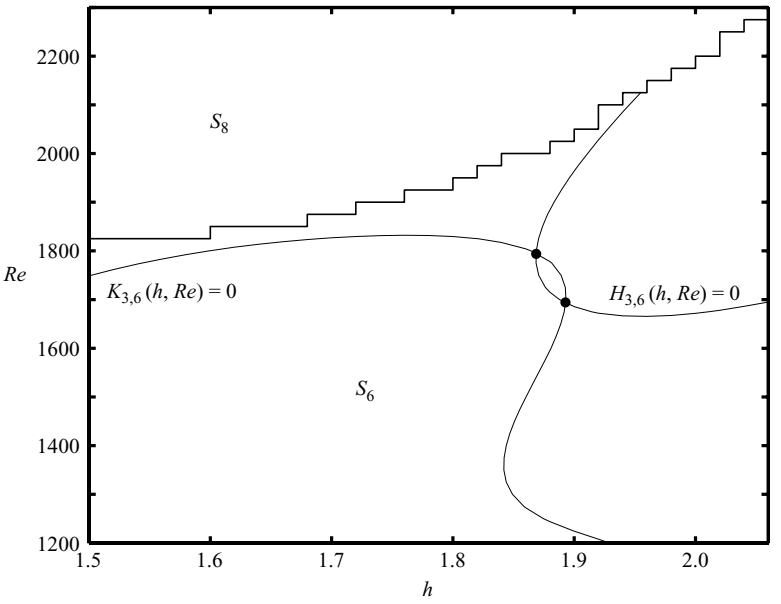

FIGURE 5. Division of the (h, Re) parameter space for $\gamma = 0.012$ into regions S_k with $k = 6$ and 8 solutions to $V'(s) = 0$. Two codimension-2 bifurcation points (filled circles) are found as intersections of the solution curves to $K_{3,6} = 0$ and $H_{3,6} = 0$.

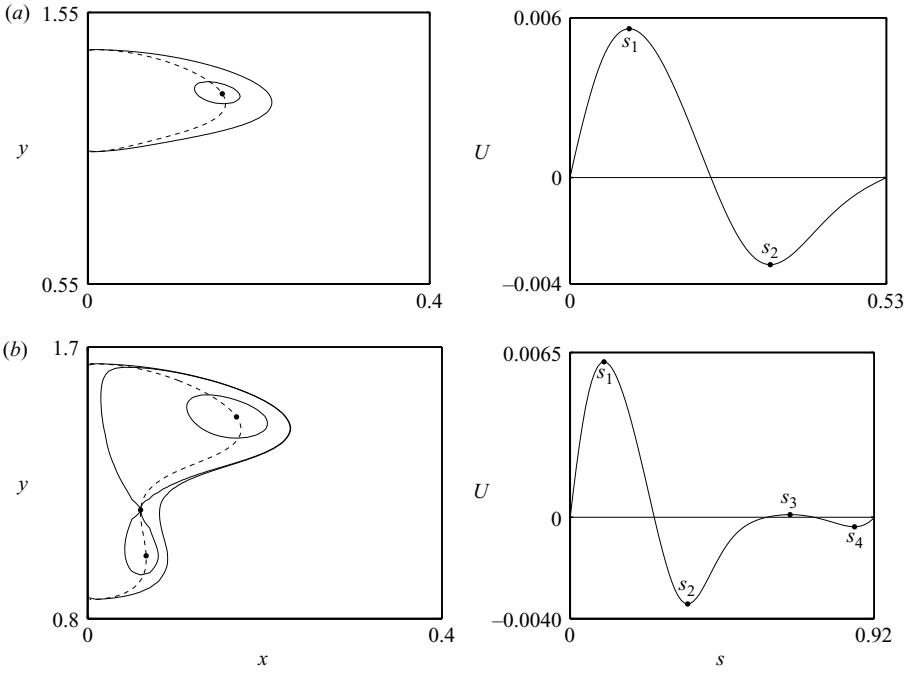

FIGURE 6. Left-hand side: a section of the flow topology with a branch of the 0-isocline shown dashed. Right-hand side: corresponding graphs of U, the u-component of the velocity along the branch. The parameter values of (a) and (b) are as in (a) and (d) in figures 3 and 4.

stagnation points. The off-axis bifurcation curve is found by solving the associated bifurcation equation $G_3(h, Re) = 0$. It is shown in figure 7 together with the on-axis bifurcation curves from figure 3 and the codimension-2 points from figure 5. No

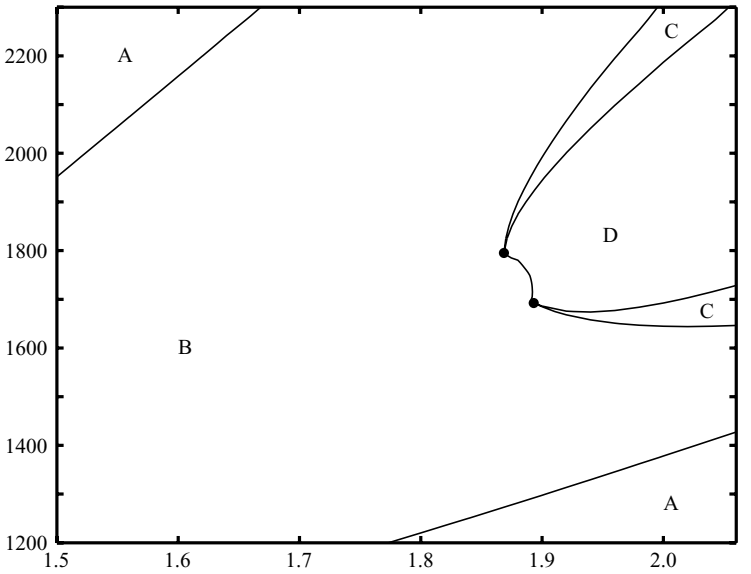

FIGURE 7. The full set of bifurcation curves and codimension-2 points for $\gamma = 0.012$. In each region, the letters denote the topology as indicated in figure 1.

other branches of the 0-isocline give rise to bifurcation, and hence the diagram is complete.

Further details on the implementation can be found in (Bisgaard 2005).

5. Comparison with experiments

A few experimental bifurcation diagrams are available in the literature. In figure 8, we compare results by Escudier (1984) and Roesner (1989) for $\gamma = 0$ with numerical bifurcation curves obtained with the isocline method. Excellent agreement is obtained.

Bar-Yoseph *et al.* (1990*a*) have published experimental results for non-zero rotation ratios. Their choice of dimensionless parameters are slightly different from ours, as the rotation frequencies n_1, n_2 of the fast and slow lid, respectively, are used instead of Re and γ. Since

$$n_1 = \frac{\nu}{2\pi R^2} Re, \qquad n_2 = \gamma n_{top} = \frac{\nu}{2\pi R^2} \gamma Re, \tag{18}$$

and $R = 70\,\mathrm{mm}$ and $\nu = 100\,\mathrm{mm^2\,s^{-1}}$ in the experiment (Roesner, personal communication 2005), transformation between the two sets of dimensionless parameters is easily achieved. Using this, the bifurcation diagram in figure 9 is obtained. Again, good agreement is found.

6. Bifurcation diagrams in the range $-0.04 \leqslant \gamma \leqslant 0.075$

6.1. *Theoretical framework from bifurcation theory*

Before we embark on the numerical study of topological bifurcations for the flow in the cylinder, we briefly review the relevant bifurcation theory to clarify which changes in the flow structure can be expected.

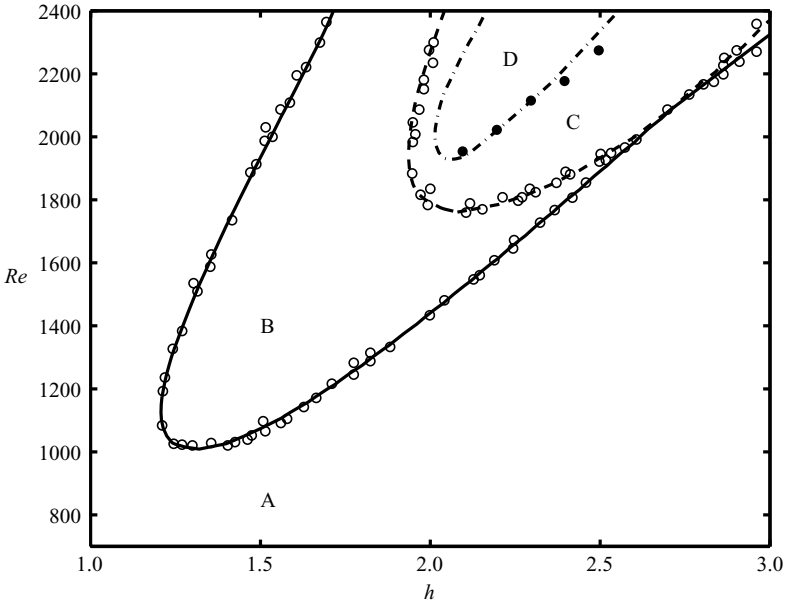

FIGURE 8. Computational bifurcation diagram for $\gamma = 0$ compared with experiments by Escudier (1984) (open circles) and Roesner (1989) (closed circles).

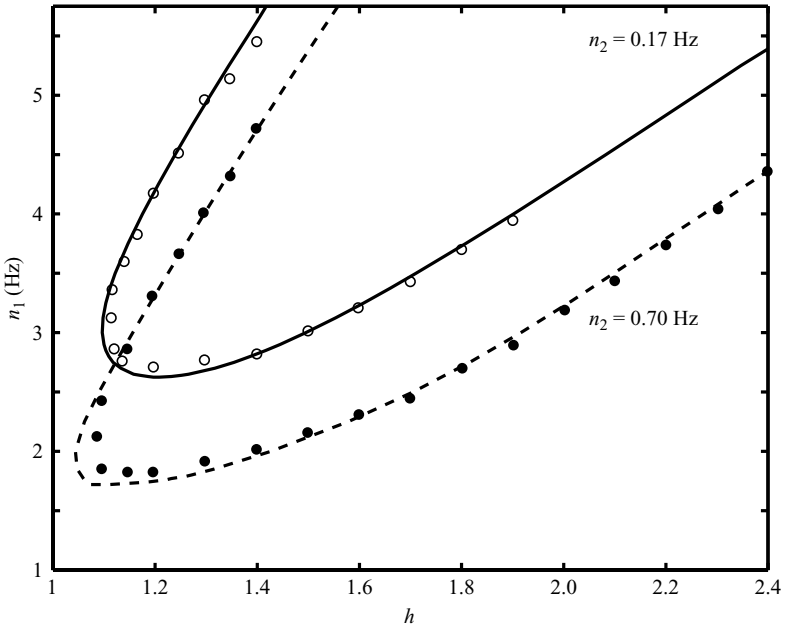

FIGURE 9. Computational bifurcation diagram for non-zero rotation ratios compared with experiments (open and closed circles) by Bar-Yoseph *et al.* (1990*a*). Below the curves there are no bubbles, above the curves a single bubble exists.

As we have three independent parameters, h, Re, γ, at our disposal we are able to fulfil up to three degeneracy conditions. Hence, we expect to see bifurcation phenomena of codimension up to 3, as described in § 3. Local topological bifurcations

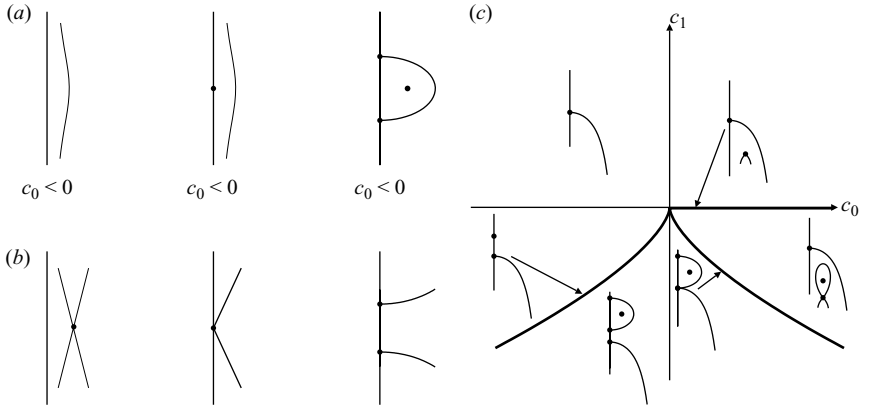

FIGURE 10. Topological bifurcation diagrams for the normal form (19). (*a*) Codimension 1, $\sigma = +1$, bubble creation. (*b*) Codimension 1, $\sigma = -1$, bubble merging. (*c*) Codimension 2.

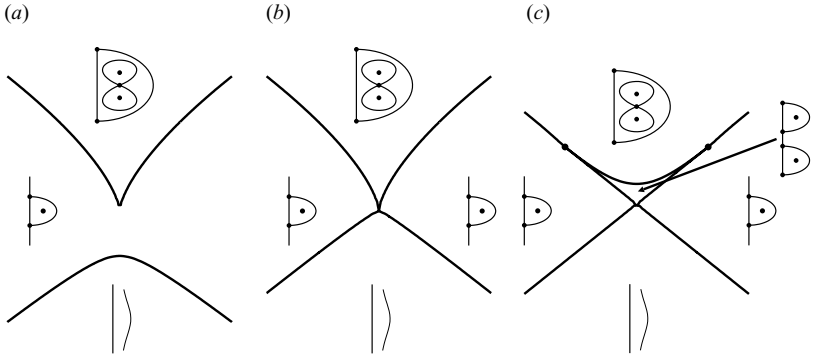

FIGURE 11. Regular codimension-3 scenario for the normal form (19) with $\sigma = +1$. The bifurcation diagrams are shown in planes of the form $c_1 + c_2 + \alpha = 0$. (*a*) $\alpha < 0$. (*b*) $\alpha = 0$. (*c*) $\alpha > 0$. As α is increased, a curve of cusp bifurcations meets a curve of bubble creation bifurcations. This gives rise to two codimension-2 points and a further curve of bubble merging bifurcations.

are associated with the occurrence of degenerate stagnation points as in figure 2(*b*). The degeneracy is *simple* if the linearization of the differential equations for the streamlines, equation (3), has zero as an eigenvalue of geometric multiplicity 1. For this case, for the flow close to the cylinder axis, Brøns (1999) derives a normal form for the stream function of codimension N,

$$\psi = x\left(\tfrac{1}{2}\sigma x + c_0 + c_1 y + \cdots + c_{N-1}y^{N-1} + \frac{1}{N+1}y^{N+1}\right). \tag{19}$$

Here the c_i are transformed free parameters, and $\sigma = \pm 1$ is the sign of a certain non-degenerate parameter. The factor x reflects that the axis $x = 0$ is a streamline. The degenerate stagnation point of codimension N occurs for $c_0 = \cdots = c_{N-1} = 0$. The bifurcation structure of (19) is shown in figures 10 and 11.

There are two types codimension-1 bifurcation, *bubble creation* (figure 10*a*) and *bubble merging* (figure 10*b*). For even codimensions, the bifurcation diagram does not depend on the sign of σ, so for $N = 2$ there is only one diagram (figure 10*c*). Here a curve of bubble creation, a curve of bubble merging, and a curve of off-axis cusp

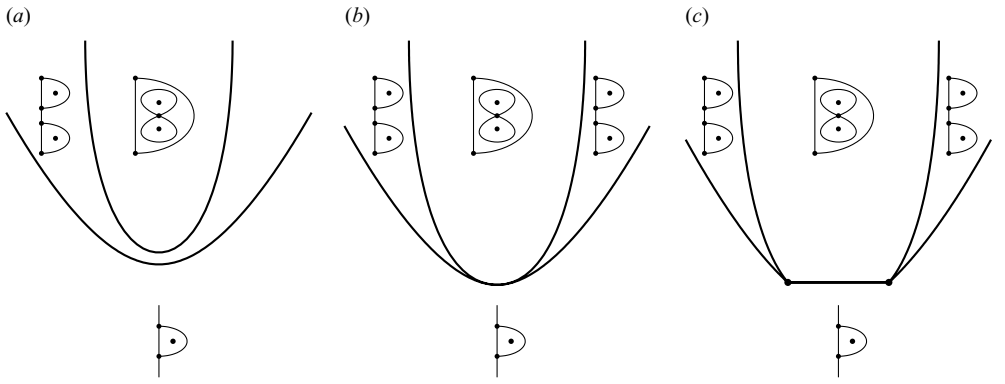

FIGURE 12. The folded codimension-3 scenario in the (h, Re) parameter plane. (*a*) $\gamma < \gamma^*$. (*b*) $\gamma = \gamma^*$. (*c*) $\gamma > \gamma^*$. As γ is increased, a curve of bubble creation and a curve of bubble merging bifurcations meet and give rise to two codimension-2 points and a curve of cusp bifurcations.

bifurcations emanate from the codimension-2 point. In the cusp bifurcation, off-axis stagnation points are created or destroyed as shown in figure 2.

The codimension-3 case can be displayed in several different ways as a sequence of two-parameter bifurcation diagrams. One such choice is shown in figure 11 for $\sigma = +1$. Later we will see that exactly this sequence will appear in the cylinder flow. The $\sigma = -1$ case does not occur, so we omit it here.

The bifurcation diagrams in figure 11 show slices in the three-dimensional space of transformed parameters c_1, c_2, c_3. These will depend on the physical parameters, in our case h, Re, γ. If the relation between the two sets of parameters is regular, that is, there is a bijective mapping between them, the bifurcation diagrams will also occur in the physical parameter space. We denote this codimension-3 scenario *regular*. However, a codimension-3 situation may also occur if there is a degeneracy in the relation between the mathematical and physical parameters. For example, suppose that a codimension-2 bifurcation, stemming from two degeneracy conditions, occurs at some (h^*, Re^*, γ^*). Then the local streamline structure is described by (19) with $N = 2$, and the two free parameters c_0, c_1. If, say,

$$\frac{\partial c_0}{\partial h}(h^*, Re^*, \gamma^*) = 0, \tag{20}$$

a third degeneracy condition appears. The bifurcation structure associated with these degeneracies is treated by Brøns (2006), and gives rise to the bifurcation diagrams shown in figure 12. We can think of this as the physical parameter plane (h, Re) being folded along a line and placed in the (c_1, c_2) parameter space of figure 10(*c*). Varying γ corresponds to moving the fold line through the codimension-2 point at the origin. Hence, we denote this the *folded* codimension-3 scenario.

For the flow in the cylinder we expect to find, in the three-dimensional parameter space, surfaces of codimension-1 bifurcations, curves of codimension-2 bifurcations, and isolated points of codimension 3. Consequently, for the two-dimensional slices for constant γ, we expect to find curves of codimension-1 bifurcations, points of codimension-2 bifurcations, and no bifurcations of codimension 3 except at special, isolated values of γ.

This is indeed what we see in figure 7. There are two codimension-2 points from each of which three codimension-1 curves emanate. The structure of the

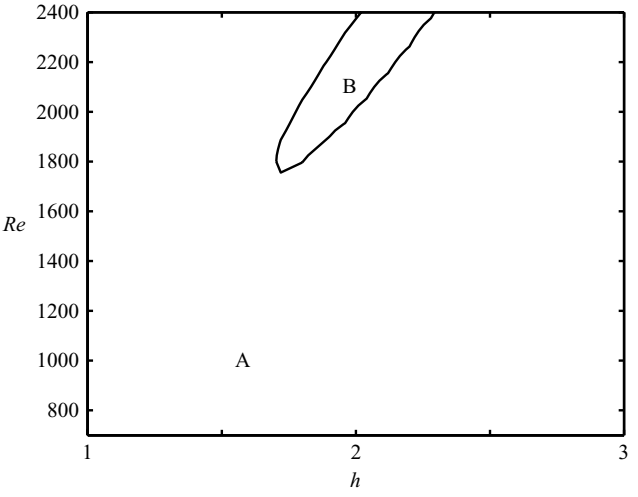

FIGURE 13. Bifurcation diagram for $\gamma = -0.04$.

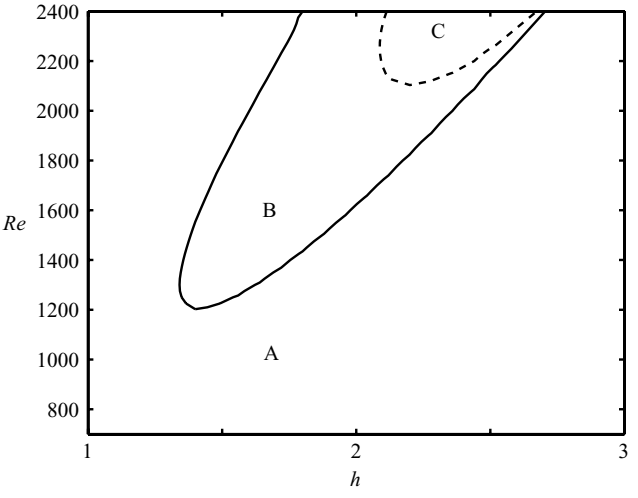

FIGURE 14. Bifurcation diagram for $\gamma = -0.02$.

bifurcation diagram close to the codimension-2 points is as in figure 10(c), as expected. Furthermore, there are two other codimension-1 curves. Hence, the theoretical bifurcation diagrams act as local building blocks for the complete diagram.

6.2. *Bifurcation diagrams*

Using the method described in § 4 we show in figures 13 to 21 topological bifurcation diagrams in the (h, Re)-plane for $-0.04 \leqslant \gamma \leqslant 0.075$. In all figures, a full line denotes bubble creation bifurcation, a dashed line a second bubble creation bifurcation, a dash-dotted line a bubble merging bifurcation, and a dotted line cusp bifurcation off the axis.

For $\gamma = -0.04$, figure 13, only a single curve of bubble creation bifurcation is present with a small parameter region where a single bubble exists. Increasing γ to -0.02, figure 14, the bubble creation curve moves further into the diagram, and yet a bubble creation curve appears. For $\gamma = 0$, figure 15, a curve of bubble merging

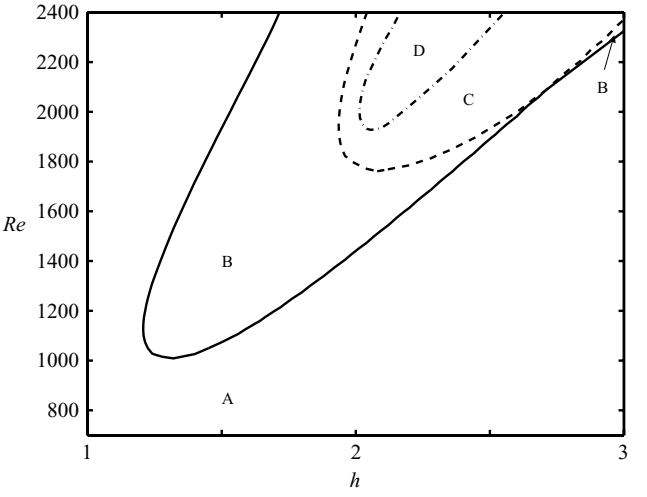

FIGURE 15. Bifurcation diagram for $\gamma = 0$.

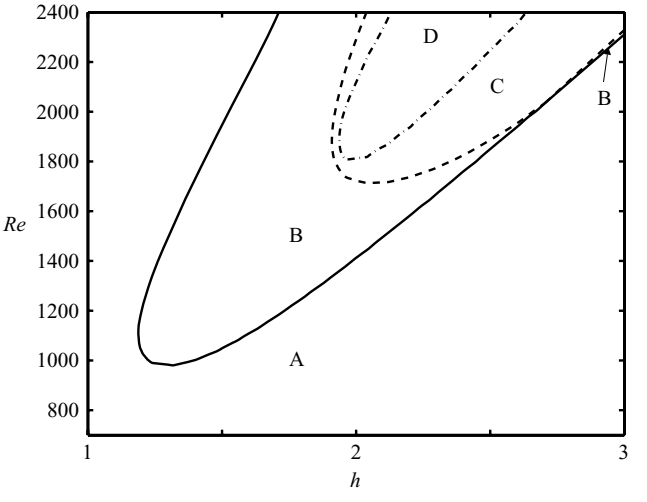

FIGURE 16. Bifurcation diagram for $\gamma = 0.005$.

bifurcations occurs, and in this diagram all four flow topologies from figure 1 are present. All three bifurcation curves are created outside the parameter region we consider, probably in the unsteady regime, and move continuously into the diagram for increasing values of γ. We have not monitored the exact values of γ where the curves enter the steady regime.

For $\gamma = 0.005$, figure 16, the bifurcation diagram is qualitatively unchanged, but the second bubble creation curve and the bubble merging curve have moved closer together. This indicates the bifurcation scenario shown in figure 12 will appear. Indeed, increasing γ to 0.012, figure 17, we see that the two codimension-1 bifurcation curves meet in codimension-2 points a and b and a curve of cusp bifurcations connect these points. Hence, for some $\gamma^{(1)} \in]0.005, 0.012[$ a codimension-3 point of folded type exists (with $h^{(1)} \approx 1.8$, $Re^{(1)} \approx 1700$).

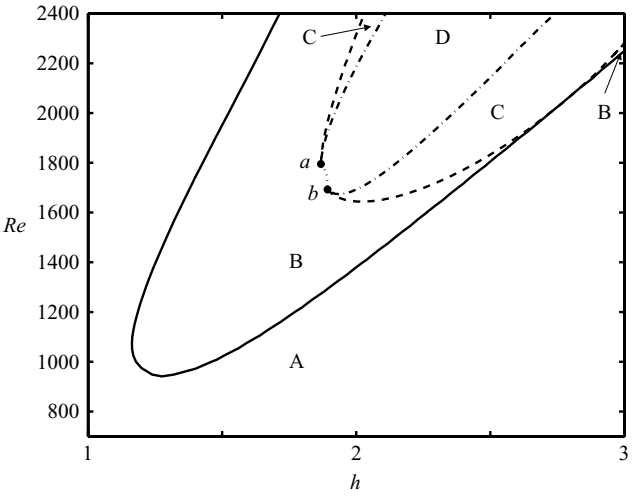

FIGURE 17. Bifurcation diagram for $\gamma = 0.012$.

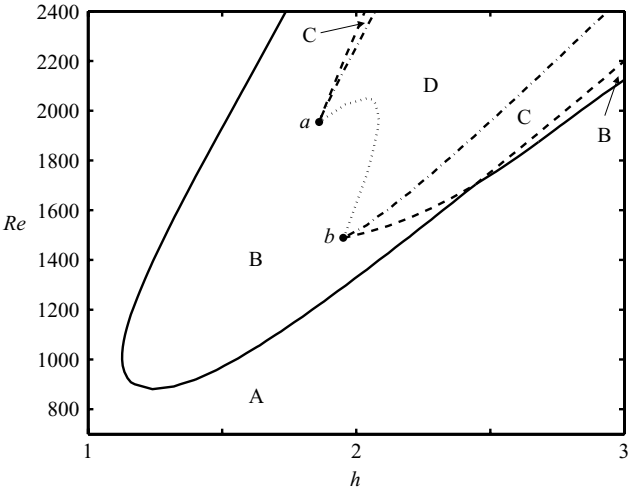

FIGURE 18. Bifurcation diagram for $\gamma = 0.03$.

Increasing γ to 0.03, figure 18, gives no qualitative change in the bifurcation diagram. The codimension-2 points have moved away from each other, and the curve of cusp bifurcations now turns upwards, making the region with one breakdown bubble considerably larger. This tendency continues as γ is increased. For $\gamma = 0.065$, figure 19, point a has moved almost out of the diagram, and b is now very close to the first bubble creation curve. Thus, there is a region with four bifurcation curves being very close, as shown in the enlargement in figure 19.

A small increment in γ to 0.0675 (figure 20) results in a qualitative change. To new codimension-2 points c and d have appeared. They are created in a folded codimension-3 bifurcation for some $\gamma^{(2)} \in]0.065, 0.0675[$ where the second bubble creation curve and the bubble merging curve touch tangentially, and again the sequence in figure 12 occurs.

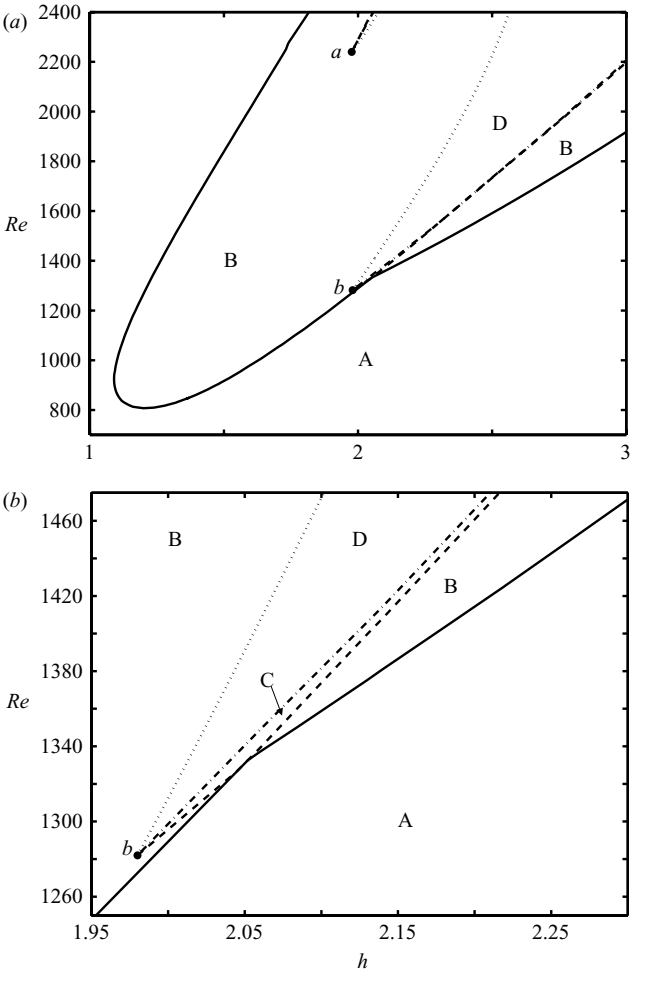

FIGURE 19. Bifurcation diagram for $\gamma = 0.065$. (*b*) An enlargement of the region close to the codimension-2 point *b*.

The region near *b* and *c* is shown in an enlargement in figure 20. Note that the qualitative structure of this diagram is exactly as in figure 11(*c*). As we increase γ to 0.075 (figure 21) we see that the bifurcation diagram has changed to that of figure 11(*a*). Thus, for some $\gamma^{(3)} \in]0.0675, 0.075[$ a regular codimension-3 point must be present. The codimension-2 points *b* and *c* have merged and disappeared in the bifurcation. Also the codimension-2 points *a* and *d* have moved out of the diagram.

7. Conclusions

In the present paper, we have obtained numerical topological bifurcation diagrams for the flow structure of vortex breakdown in a circular cylinder with two rotating covers. We interpret the diagrams with the aid of bifurcation theory, which gives a high degree of certainty that the bifurcation diagrams are complete. Bifurcation theory gives precise conditions on the velocity field and its derivatives for changes of the flow patterns to occur. These conditions are difficult to interpret in simple

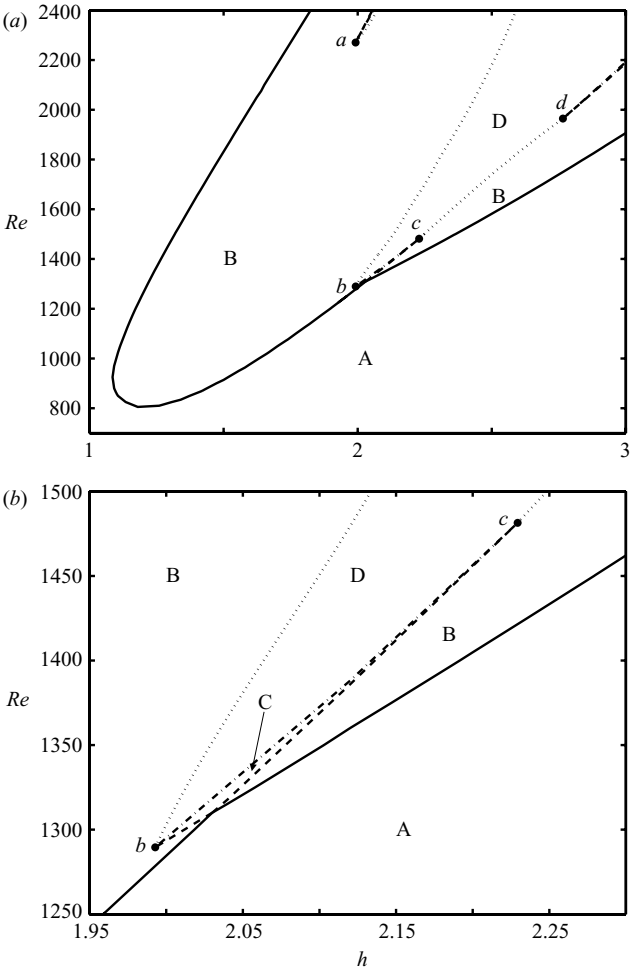

FIGURE 20. Bifurcation diagram for $\gamma = 0.0675$. (*b*) An enlargement of the region close the codimension-2 points *b* and *c*.

physical terms, and only a mathematical treatment of data, as in the present study, can give the desired results.

The diagrams confirm that counter-rotating covers suppress vortex breakdown whereas co-rotating covers have the opposite effect (Valentine & Jahnke 1994; Mununga *et al.* 2005). Furthermore, for positive values of the rotation rate γ, we see a fundamental transition of the diagrams as γ is increased. For γ very close to 0, two bubbles are present in a rather large parameter region, but this topology does not occur at all for higher values of γ. At the same time, the parameter region with one bubble with an inner structure becomes more prominent. This transition takes place in the narrow range $0 \leqslant \gamma \leqslant 0.075$ through a rather complex sequence of topological bifurcations, involving three codimension-3 points. These points in the parameter space are associated with degenerate stagnation points on the cylinder axis, and the local bifurcation structure is completely described by the normal form (19) which accounts for bifurcations taking place close to the cylinder axis. At higher values of γ than considered here, bifurcations which are not local to the axis will occur, and will

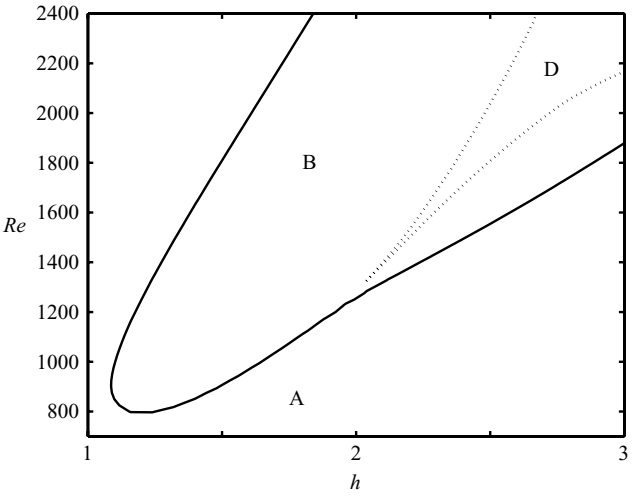

FIGURE 21. Bifurcation diagram for $\gamma = 0.075$.

require different normal forms for their interpretation (Bisgaard, Brøns & Sørensen 2006). The numerical procedure is, however, independent of this, and will apply in general.

We have developed the isocline method as a general means of obtaining topological bifurcation diagrams and applied it to the flow in the cylinder. Elements of the method was applied in previous studies of the flow in the cylinder (Brøns *et al.* 1999, 2001), where global quadratic approximations to the bifurcation curves were found by a manual procedure which cannot be expected to be generally applicable. As we are considering the bifurcations of patterns of the trajectories of a two-dimensional system of ordinary differential equations (3) under variation of parameters, there are of course many well-established alternatives available for solving this fundamental problem in non-linear dynamics. A number of packages based on path-following exist, with AUTO (Doedel *et al.* 1997) as one of the most popular; but for topological problems in fluid mechanics, path-following may be very cumbersome. The bifurcation curves are constructed in steps, and for each step some iteration procedure is required to find the correct point from an initial guess. As each new set of parameters will require a new simulation of the Navier–Stokes equations and as the required steps will typically be very small, in particular when bifurcation diagrams are complex as is the case here, this may in our experience be very time-consuming, requiring substantial user interaction. The programs require an analytical expression for the velocity field to locate the stagnation points, and when the field is only given numerically, some interpolation must be performed in each step, making the interface between the Navier–Stokes solver and the path-following program a non-trivial matter. In contrast, the isocline method starts with a database of simulations and then gives the bifurcation diagrams by post-processing.

The isocline method can also easily be configured to give successive refinements of the bifurcation diagram. One may start with a few simulations on a very coarse grid in the parameter space, and use these data to form a rough idea of the bifurcation diagram, as the bifurcation functions G, whose zeros are the bifurcation curves, are well-defined on any grid. The grid may then be refined adaptively in the regions where bifurcations occur until the desired resolution is achieved. For simplicity, we have not

applied this strategy in the present paper, but we consider it an important asset of the method. A similar feature is hard to implement in a path-following method. Hence, the isocline method has the potential to be an efficient tool for generating topological bifurcation diagrams for general two-dimensional flows.

J. N. Sørensen has kindly provided us with the axisymmetric solver *czax* which we have used for the numerical simulations. We thank an anonymous reviewer for pointing out the paper by Bar-Yoseph *et al.* (1990*a*).

REFERENCES

Bar-Yoseph, P., Solan, A. & Roesner, K. G. 1990*a* Numerical simulation and experimental verification of cavity flows. In *The Navier–Stokes Equations. Theory and Numerical Methods* (ed. J. G. Heywood, K. Masuda, R. Rautmann & V. A. Solonnikov), Lecture Notes in Mathematics, vol. 1431, pp. 229–235. Springer.

Bar-Yoseph, P. Z., Solan, A. & Roesner, K. G. 1990*b* Sekundärströmung in axialsymmetrichen Hohlräumen. *Z. Angew. Math. Mech.* **70**, 442–444.

Bisgaard, A. V. 2005 Structures and bifurcations in fluid flows with applications to vortex breakdown and wakes. PhD thesis, Department of Mathematics, Technical University of Denmark.

Bisgaard, A. V., Brøns, M. & Sørensen, J. N. 2006 Vortex breakdown generated by off-axis bifurcation in a circular cylinder with rotating covers. *Acta Mech.* (to appear).

Brøns, M. 1999 Topological fluid mechanics of axisymmetric flows. In *Simulation and Identification of Organized Structures in Flows* (ed. J. N. Sørensen, E. J. Hopfinger & N. Aubry), Kluwer.

Brøns, M. 2006 Streamline topology – patterns in fluid flows and their bifurcations. *Adv. Appl. Mech.* **41** (in press).

Brøns, M. & Bisgaard, A. 2004 Bifurcation of vortex breakdown patterns. In *Proc. 2004 International Conference on Computational & Experimental Engineering & Sciences* (ed. S. N. Atluri & A. J. B. Tadeu), pp. 988–993. Tech Science Press, Georgia, USA.

Brøns, M. & Hartnack, J. N. 1999 Streamline topologies near simple degenerate critical points in two-dimensional flow away from boundaries. *Phys. Fluids* **11**, 314–324.

Brøns, M., Voigt, L. K. & Sørensen, J. N. 1999 Streamline topology of steady axisymmetric vortex breakdown in a cylinder with co- and counter-rotating end-covers. *J. Fluid Mech.* **401**, 275–292.

Brøns, M., Voigt, L. K. & Sørensen, J. N. 2001 Topology of vortex breakdown bubbles in a cylinder with a rotating bottom and a free surface. *J. Fluid Mech.* **428**, 133–148.

Daube, O. 1991 Numerical simulations of axisymmetric vortex breakdown in a closed cylinder. In *Vortex Dynamics and Vortex Methods* (ed. C. R. Anderson & C. Greengard). *Lectures in Applied Mathematics*, vol. 28, pp. 131–152. American Mathematical Society.

Daube, O., Loc, T. P., Monet, P. & Coutanceau, M. 1985 Ecoulement instationaire décollé d'un fluide incompressible autour d'un profil: une comparaison theorié–experience. AGARD CP 366.

Doedel, E., Champneys, A. R., Fairgrieve, T. F., Kuznetsov, Y. A., Sandstede, B. & Wang, X. 1997 AUTO 97: Continuation and bifurcation software for ordinary differential equations (with HomCont). Tech. Rep. Concordia Unversity.

Dusting, J., Sheridan, J. & Hourigan, K. 2004 Flows within a cylindrical cell culture bioreactor with a free-surface and a rotating base. In *Proc. of the 15th Australasian Fluid Mechanics Conference* (ed. M. Behnia, W. Lin & G. D. McBain). University of Sydney.

Escudier, E. P. 1984 Observations of the flow produced in a cylindrical container by a rotating end wall. *Exps. Fluids*, **2**, 189–196.

Gelfgat, A. Y., Bar-Yoseph, P. Z. & Solan, A. 1996*a* Steady states and oscillatory instability of swirling flow in a cylinder with rotating top and bottom. *Phys. Fluids* **8**, 2614–2625.

Gelfgat, A. Y., Bar-Yoseph, P. Z. & Solan, A. 1996*b* Stability of confined swirling flow with and without vortex breakdown. *J. Fluid Mech.* **311**, 1–36.

Gelfgat, A. Y., Bar-Yoseph, P. Z. & Solan, A. 2001 Three-dimensional instability of axisymmetric flow in a rotating lid–cylinder enclosure. *J. Fluid Mech.* **438**, 363–377.

Hartnack, J. N., Brøns, M. & Spohn, A. 2000 The role of asymmetric perturbations in steady vortex breakdown bubbles. DCAMM Rep. 628, Technical University of Denmark.

Herrada, M. A. & Shtern, V. 2003 Control of vortex breakdown by temperature gradients. *Phys. Fluids* **15**, 3468–3477.

Lopez, J. M. 1990 Axisymmetric vortex breakdown. Part 1. Confined swirling flow. *J. Fluid Mech.* **221**, 533–552.

Mununga, L., Hourigan, K., Thompson, M. C. & Leweke, T. 2005 Confined flow vortex breakdown control using a small rotating disk. *Phys. Fluids* **16**, 4750–4753.

Okulov, V. L., Sørensen, J. N. & Voigt, L. K. 2005 Vortex scenario and bubble generation in a cylindrical cavity with rotating top and bottom. *Eur. J. Mech. Fluids* B **24**, 137–148.

Roesner, K. G. 1989 Recirculation zones in a cylinder with rotating lid. *Proc. IUTAM Symposium on Topological Fluid Mechanics* (ed. A. Tsinober & H. K. Moffatt), pp. 699–708.

Ronnenberg, B. 1997 Ein Selbstjustierendes 3-komponenten-Laserdoppler-anemometer nach dem Vergleichsverfaren, angewandt auf Untersuchungen in einer stationären zylindersymmetrischen Drehströmung mit enimen Rückströmgebiet. *Bericht 19*. Max-Planck Institut für Strömungsforshung, Göttingen.

Sørensen, J. N. & Christensen, E. A. 1995 Direct numerical simulation of rotating fluid flow in a closed cylinder. *Phys. Fluids* **7**, 764–778.

Sørensen, J. N. & Loc, T. P. 1989 Higher-order axisymmetric Navier–Stokes code: description and evaluation of boundary conditions. *Intl J. Numer. Meth. Fluids* **9**, 1517–1537.

Sotiropoulos, F. & Ventikos, Y. 2001 The three-dimensional structure of confined swirling flows with vortex breakdown. *J. Fluid Mech.* **426**, 155–175.

Spohn, A., Mory, M. & Hopfinger, E. J. 1998 Experiments on vortex breakdown in a confined flow generated by a rotating disc. *J. Fluid Mech.* **370**, 73–99.

Thompson, M. C. & Hourigan, K. 2003 The sensitivity of steady vortex breakdown bubbles in confined cylinder flows to rotating lid misalignment. *J. Fluid Mech.* **496**, 129–138.

Tsitverblit, N. 1993 Vortex breakdown in a cylindrical container in the light of continuation of a steady solution. *Fluid Dyn. Res.* **11**, 19–35.

Valentine, D. T. & Jahnke, C. C. 1994 Flows induced in a cylinder with both end walls rotating. *Phys. Fluids* **6**, 2702–2710.

Vogel, H. U. 1968 Experimentelle Ergebnisse über die laminäre Strömung in einem zylindrischen Gehäuse mit darin rotierender Scheibe. *Bericht 6*. Max-Planck-Institut für Strömungsforschung, Göttingen.

Westergaard, C., Buchhave, P. & Sørensen, J. N. 1993 PIV measurements of turbulent and chaotic structures in a rotating flow using an optical correlator. *Laser Techniques and Applications in Fluid Mechanics* (ed. R. J. Adrian). Springer.

Wiggins, S. 2003 *Introduction to Applied Nonlinear Dynamical Systems and Chaos*, 2nd edn. Springer.